Local Group Satellite Distributions in the Illustris Simulation

Jaime E. Forero-Romero [1] ⋆, Verónica Arias[1]

[1] *Departamento de Física, Universidad de los Andes, Cra. 1 No. 18A-10 Edificio Ip, CP 111711, Bogotá, Colombia*

20 October 2017

ABSTRACT

We quantify the joint spatial distribution of satellites around the Milky way and Andromeda.

Key words: Galaxies: halos — Galaxies: high-redshift — Galaxies: statistics — Dark Matter — Methods: numerical

1 INTRODUCTION

In Section we list the sources of the observatinal and simulated data to be used throughout the paper. Next, in Section we describe the methods we use to quantify and characterize the satellite distributions. In section we present our results. First we describe the observed satellite distributions and compare them against the expectation of an spherical randomization of its satellites. We then compute the expectation from the Illustris Simulation. In Section we discuss the implication of our results to finally summarize in Section.

2 OBSERVATIONAL DATA

3 LOCAL GROUP SATELLITES IN THE ILLUSTRIS SIMULATION

We use publicly available data from the Illustris Project (Vogelsberger et al. 2014). This suite of cosmological simulations, performed using the quasi-Lagrangian code AREPO (Springel 2010), followed the coupled evolution of dark matter and gas and includes parametrizations to account for the effects of gas cooling, photoionization, star formation, stellar feedback, black hole and super massive black hole feedback. The simulation volume is a cubic box of 75 Mpc h^{-1} on a side. The cosmological parameters correspond to a ΛCDM cosmology consistent with WMAP-9 measurements (Hinshaw et al. 2013).

We extract halo and galaxy information from the Illustris-1 simulation which has the highest resolution in the current release of the Illustris Project. Illustris-1 has 1820^3 dark matter particles and 1820^3 initial gas volumen elements. This corresponds to a dark matter particle mass of $6.3 \times 10^6 M_\odot$ and a minimum mass for the baryonic volume

⋆ je.forero@uniandes.edu.co

element of $8.0 \times 10^7 M_\odot$. The corresponding spatial resolution is 1.4 kpc for the dark matter gravitational softening and 0.7 kpc for the typical size of the smallest gas cell size.

The smallest satellites are barely resolved in stellar mass at magnitudes of $M_V = 9$, however its dark matter structure is sampled with at least 100 particles. We find that all considered halos have at least XX subhalos above a maximum circular velocity of 15km s^{-1}. For this reason we select the satellite galaxy samples from the DM subhalo population and not from the galaxies with photometry. We chose in two different ways the sub-halo samples. First, we rank the halos by decreasing order of its maximum circular velocity and select the first N_p halos in the list. Second, we select all satellites above maximum circular velocity of 20km s^{-1}to randmbly subsample N_p subhalos.

We build a sample of Local Group Analgues (LGA) by selecting first all galaxies with an stellar mass in the range $1 \times 10^{10} M_\odot < M_\star < 1.5 \times 10^{11} M_\odot$. Then we consider the following criteria for all galaxies in that sample.

• For each galaxy A we find its closest galaxy B, if galaxy A is also the closest to halo B, the two are considered as a pair.

• With d_{AB} the distance between the two galaxies and $M_{\star,min}$ the lowest stellar mass in the two galaxies, we discard pairs that have any other galaxy C with stellar mas $M_\star > M_{\star,min}$ closer than $3 \times d_{AB}$ from any of the pair's members.

• The distance d_{AB} greater than 700 kpc.

• The relative radial velocity between the two galaxies, including the Hubble flow, is -120 km s$^{-1} < v_{AB,r} < 0$ km s^{-1}.

We find 27 pairs with these conditions. Figure shows the physical properties (stellar masses, maximum circular velocities, radial velocities and separation) in those pairs.

4   SATELLITE SPATIAL DISTRIBUTION

We base all our results on the description provide by the inertia tensor defined by the satellites's positions.

$$\bar{\mathbf{I}} = \sum_{k \in V} [(\mathbf{r_i} - \mathbf{r_0})^2 \cdot \mathbf{1} - (\mathbf{r_i} - \mathbf{r_0}) \cdot (\mathbf{r_i} - \mathbf{r_0})^{\mathbf{T}}], \tag{1}$$

where k indexes the set of satellites of interest $\mathbf{r_k}$ are the satellites' positions, $\mathbf{r_0}$ is the location of the satelites's geometric center $\mathbf{r_0} \equiv \frac{1}{N_s} \sum_{k \in V} \mathbf{r_i}$, $\mathbf{1}$ is the unit matrix, and $\mathbf{r}^T$ is the transposed vector $\mathbf{r}$.

From this tensor we compute its eigenvalues, $\lambda_1 > \lambda_2 > \lambda_3$, and corresponding eigenvectors, $\hat{I}_1, \hat{I}_2, \hat{I}_3$. We define the size of its three ellipsoidal axis as $a = \sqrt{\lambda_1}$, $b = \sqrt{\lambda_2}$ and $c = \sqrt{\lambda_3}$.

We define $\hat{n} \equiv \hat{I}_1$ as the vector perpendicular to the planar satellite distribution. We also define the width of the planar satellite distribution, σ_p as the standard deviation of all satellite distances to the plane defined by the $\hat{n}$.

We characterize the alignment between the satellite plane and the vector connecting the two dominant galaxies as $\mu = |\hat{r}_{AB} \cdot \hat{n}|$. It has been shown that LG pair separation vector is aligned along the filaments in which they are typically embeded Forero-Romero & González (2015), the LG pairs found in pancake-like DM matter arrangements are aligned with the plane itself. Characterizing the satellite alignments with μ thus provide information about how satellites are distributed with respect to the cosmic web.

4.1   Parameter Distributions

We charaterize the μ distribution by a power law probability density distribution

$$P(\mu) = \frac{1}{\alpha} \mu^{\alpha-1}. \tag{2}$$

We estimate the α using a bayesian approach, such as that the likelihood of being α the power value given the observed values of $\{\mu_i\}$ can be written as:

$$\mathcal{L}(\alpha | \{\mu_i\}) = \frac{1}{Z_\alpha} \prod_{i=1}^{N_s} \frac{1}{\alpha} \mu_i^{\alpha-1}, \tag{3}$$

where Z_α is a constant such as $\int_0^\infty \mathcal{L}(\alpha|\{\mu_i\}) \mathrm{d}\alpha = 1$. We report as $\hat{\alpha}$ the value of α maximizing the likelihood,

We characterize the distributions for the plane width and axis ratio b/a, b/c through a gaussian

$$P(x) = \frac{1}{\sqrt{2\pi\sigma^2}} \exp\left[-\frac{1}{2}\left(\frac{x - x_m}{\sigma}\right)^2\right] \tag{4}$$

In this case the maximum likelihood values for the parameter estimates $\hat{x_m}$ and $\hat{\sigma}$ correspond to the mean and standard deviation, respectively.

We summarize the results from the Illustris simulation by reporting the maximum likelihood parameter estimates. In turn we use this us to estimate the probability of finding the observed values in the Local Group and compare it against the highest probabilty values.

4.2   Satellite samples

We compare the satellite distributions in the MW and M31 at fixed satellite number. This means that the magnitude cut corresponding to the faintest satellite included in the sample is different in each case. We make this choice for two reasons. First to always be sure that there is a non-zero number of satellites to make the computations. Second, to be able to compare the two halos at a fixed number of satellites.

We test the shape and alignment statistics for 11 up 15 satellites. The lowest number corresponds to the number of classical Milky Way satellites. The upper limit corresponds to the minimum number of satellites that can be resolved in the simulations for both halos in each pair. In the case of simulations we rank the subhalos by their maximum circular velocity. We do not use their stellar properties because this represents the lower resolution limit for the hydrodynamics; most of these subhalos only have one stellar particle belonging to them. In contrast, the detected sub-halos have at least 35 dark matter particles to determine their properties.

We build two different kinds of statistics from these satellites First, we compute the shape and alignments for a varying number of satellites $11 \leq N_s \leq 15$ keeping their ranking in M_V or V_{max}. This allows us to estimate the variation expected by changing the satellite number. The second kind of statistics are computed for a fixed number of satellites $N_s = 11$ randomly selected from the top 15 ranked satellites. We perform this bootstrapping 5 times for each pair. This allows us to estimate the variation expected by randomly sampling the satellites from a parent distribution.

5   RESULTS

5.1   Satellite distributions in the Local Group

Figure 4 summarizes our main results for the observed LG satellite distributions. We see that the Ranked and Bootstrapped samples are consistent withing the scatter provided by each sample. We use the median and standard deviation in each sample to define the most probable value and its associated uncertaintiy. This allows us to compare the observational values gainst the distributions derived from the Illustris simulation.

There is a third sample in Figure 4. It corresponds to the set of Random points generated by randomizing the angular positions of the satellites in each pair in the Bootstrapped sample. This provides a baseline to understand the importance of intrinsic satellite's radial profile distribution in driving the results.

The upper left panel in Figure 4 shows that the planar satellite distributions are located perpendicular to the line connecting the two galaxies. It is remarkable that this alignment is almost perfect for both satellite distributions. The points in the Random simply highlights the expected result for a random angular distribution is a flat distribution in the range $0 \leq \mu \leq 1$.

The upper right panel shows two interesting things. First, the MW satellite plane is thiner than its M31 counterpart. This is in principle unexpected since M31 is more massive than the MW and it should have a broader satellite distribution. The second interesting point is that the MW satellite plane is also thiner than the spherical randomized

expectation, while the M31 plane is right within the expectation of the randomized satellites. This is a another piece of evidence showing the highly structured satellite distribution in the MW in comparison to M31. The fact that the `Random` samples also show a trend towards thinner MW planes means that the radial satellite distribution in concentrated in the MW than it is in M31.

The lower left panel re-inforces the picture of a highly structured MW. It corresponds to the c/a ratio and shows the same trends observed in for the plane width. First, the ratio is lower for the MW than it is for M31; second, the ratio for the MW is also lower than the expectation for the randomized sample while the results for M31 is within the expectations from `Random`. In this case the median value of the `Random` distributions follow the $1:1$ line as expected. The lower right panel does not show any surprises. All the distributions from `Ranked`, `Bootstrapped` and `Random` are consistent both for the MW and M31.

We can quantify the degree at which the observed satellite distributions are different from their spherically randomized counterparts. Figure **??** shows the probability distributions from the `Random` pairs with an overplot of the LG values. The upper left panel shows the power law distribution for μ. The results are not perfectly horizontal because the optimal power value $\hat{alpha}$ is slightly different from 1, the uncertainties in this value are naturally consistent with the unit value expected for an homogeneous distribution. In this case all values are equiprobable. In the case of the b/a ratio (lower right panel) both the MW and M31 are consistent with the average values expected from `Random` distribution. Remarkably, the plane width and c/a ratio for the MW are significantly different from the `Random` expected values, while the M31 values are sistematically within the expectations.

The comparison of the observed satellite distribution against its onw version, but spherically randomized, tells us that the MW satellite planar structure is remarkably different from a random distribution, while for the M31 distribution there isn't a significant difference from the random expectation.

5.2 Satellite distributions in the Illustris Simulation

In the previous section we saw how the MW cannot be concealed with its randomized satellite distribution, while M31 is fully consistent with it. We now quantify whether the MW and M31 are consistent with the expectations from the Illustris Simulation. We show here the results from the `Ranked` sample. The results from the `Bootstrapped` sample ara avaialble in the appendix.

REFERENCES

Forero-Romero J. E., González R., 2015, ApJ, 799, 45
Hinshaw G., et al., 2013, ApJS, 208, 19
Springel V., 2010, MNRAS, 401, 791
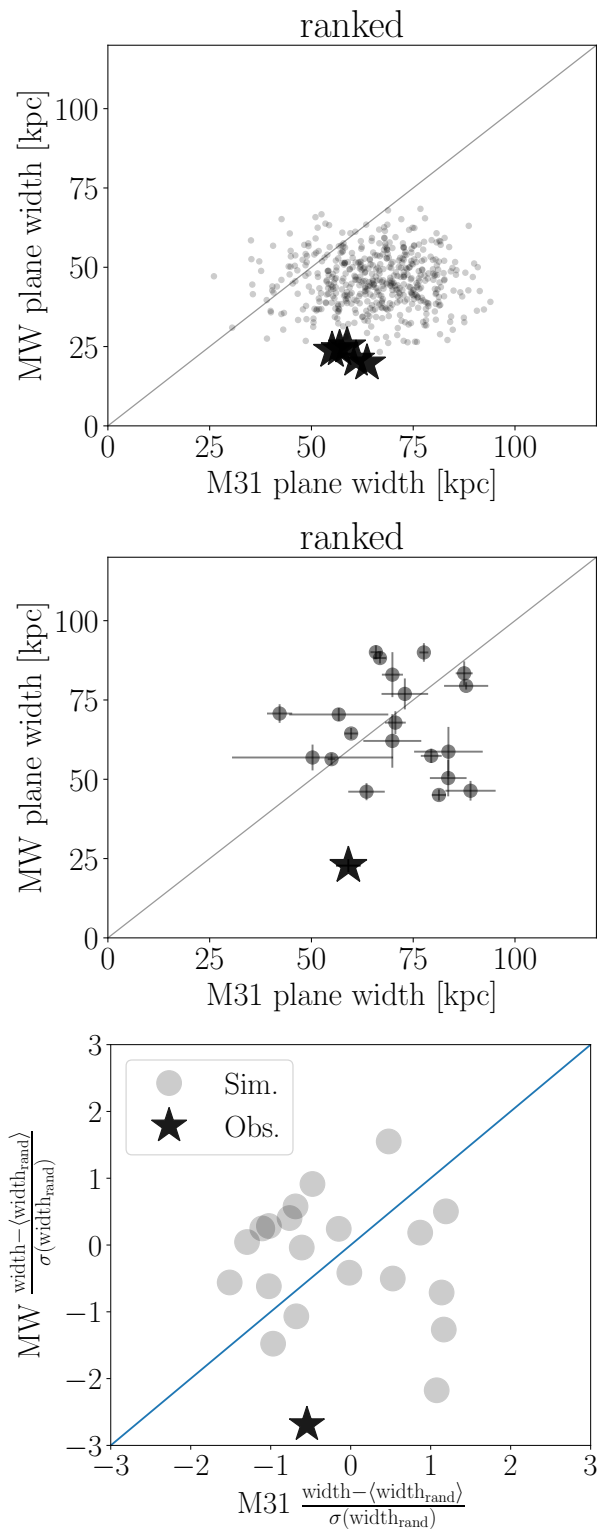Vogelsberger M., et al., 2014, MNRAS, 444, 1518

Figure 1. Basic characteristics for the MW and M31 satellite systems

Symbol	Units	Description
$\hat{r}_{AB}$		Unit vector along the direction connecting two dominant galaxies
N_s		Number of satellites
$a > b > c$	kpc	Inertia tensor eigenvalues.
$\hat{I}_1,\ \hat{I}_2,\ \hat{I}_3$		Inertia tensor eigenvectors.
σ_s	kpc	Ellipsoid width

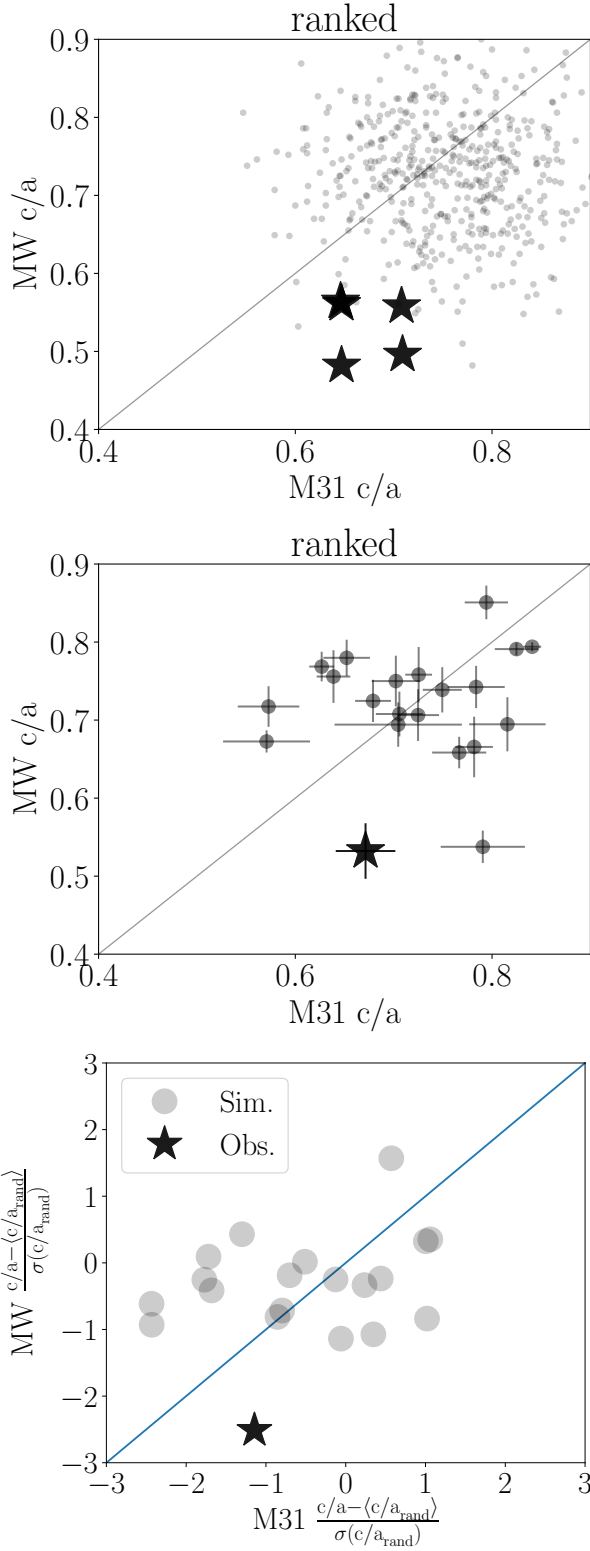**Table 1.** Overview of the parameters computed for each central galaxy and its satellite system.

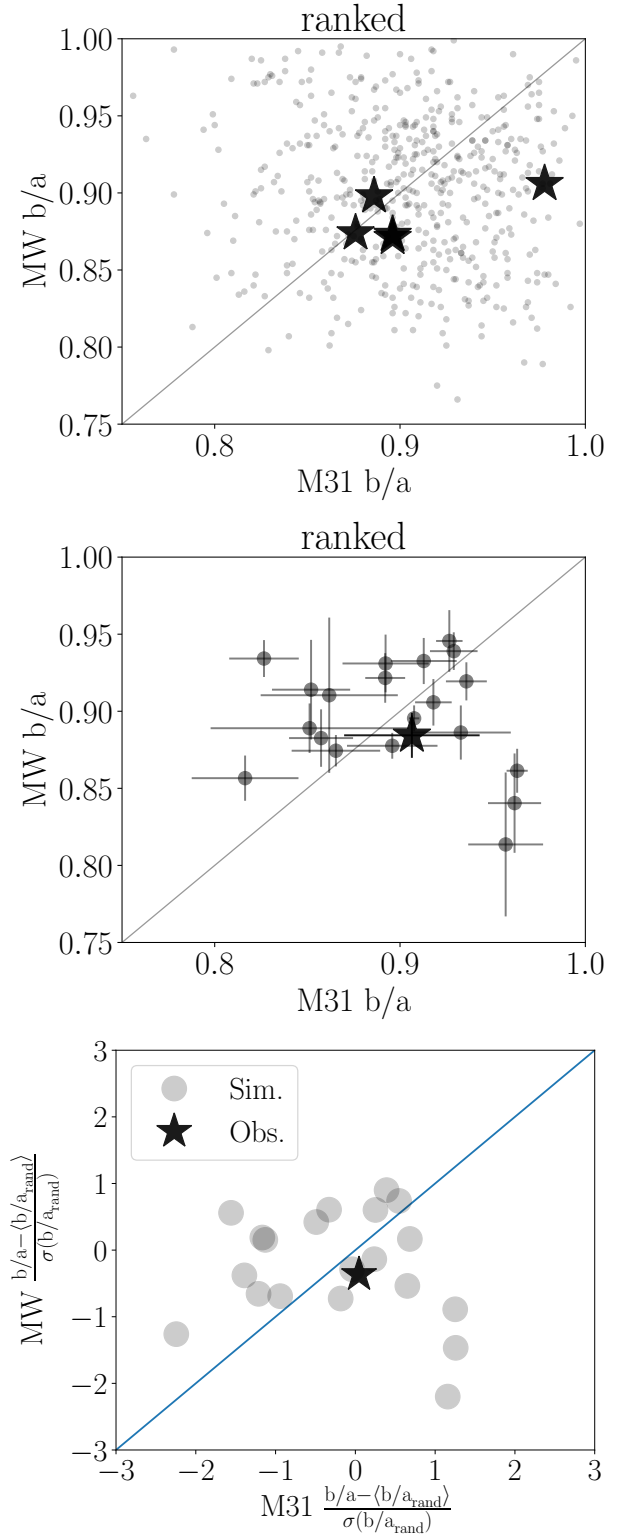**Figure 2.** Basic characteristics for the MW and M31 satellite systems

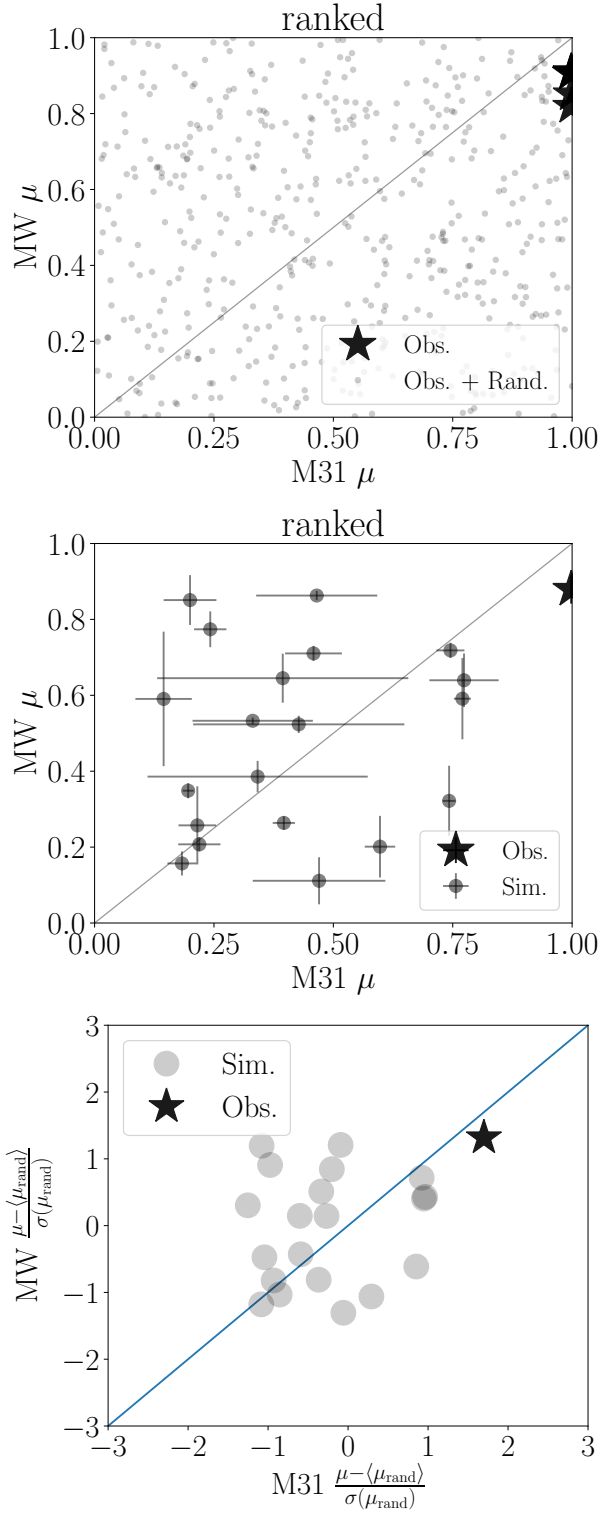**Figure 3.** Basic characteristics for the MW and M31 satellite systems

Figure 4. Basic characteristics for the MW and M31 satellite systems